NACA

RESEARCH MEMORANDUM

INVESTIGATION OF TWO-STAGE COUNTERROTATING COMPRESSOR

II - FIRST-ROTOR BLADE-ELEMENT PERFORMANCE

By Linwood C. Wright and Ward W. Wilcox

Lewis Flight Propulsion Laboratory
Cleveland, Ohio

NATIONAL ADVISORY COMMITTEE
FOR AERONAUTICS

WASHINGTON

October 5, 1956

NACA RM E56G09

NATIONAL ADVISORY COMMITTEE FOR AERONAUTICS

RESEARCH MEMORANDUM

INVESTIGATION OF TWO-STAGE COUNTERROTATING COMPRESSOR

II - FIRST-ROTOR BLADE-ELEMENT PERFORMANCE

By Linwood C. Wright and Ward W. Wilcox

SUMMARY

The blade-element performance of a highly loaded transonic rotor with double-circular-arc blades is analyzed. This rotor, which was designed by means of the conventional blade-element procedure as the first stage of a two-stage counterrotating compressor, was purposely loaded beyond the prudent level for exploratory purposes. In addition to the conventional blade-element parameters obtained from steady-state measurements, the element blade-to-blade loss distributions computed from hot-wire measurements are presented. These data allow qualitative identification of the basic independent sources of the blade-row losses.

The usual blade-element parameters, with the possible exception of the deviation angle, vary with incidence angle in a very conventional manner despite the high loading and Mach number.

Data from a previous report showing the variation of the difference between the minimum-loss incidence angle and the choking incidence angle at Mach 1.0 with relative inlet Mach number are extended herein.

INTRODUCTION

The over-all performance of a highly loaded high Mach number transonic rotor is presented in reference 1. The blade-element performance of this rotor is of particular interest because of the current concern as to the adequacy of the simple element approach to the design of rotors at high Mach numbers and work levels. In the simple element design procedure, a conical stream surface of revolution is generally assumed for the fixed design requirements and rotor-inlet and -outlet computations; the prescribed blade section is then applied on the stream surface of revolution.

This approach, which has been successful for moderately loaded transonic rotors, presumes that no important effects result from radial flows

between the rotor-inlet and -outlet stations. Moreover, the empirical relations and coefficients from which the blade sections themselves are derived may not be extensive enough to allow general consideration of all the factors (e.g., surface Mach number and shock effects) affecting blade performance at high speeds.

In order to illustrate and evaluate the performance characteristics in the high-pressure-ratio, high Mach number range of a rotor composed of double-circular-arc blade sections and designed on the conventional element basis, the detailed performance of the first rotor (ref. 1) of a two-stage counterrotating unit is presented. This detailed performance includes the radial variation of several performance characteristics and most of the conventionally presented element performance curves, along with some blade relative total-pressure-recovery plots obtained from high-frequency hot-wire measurements. These hot-wire results allow at least a qualitative identification of the basic sources of loss. In addition, empirical curves first presented in reference 2 to correlate the best blade incidence angle with the blade geometry and the relative inlet Mach number are extended from the current data and presented herein.

414/

SYMBOLS

A_F compressor frontal area based on inlet tip diameter, sq ft

D diffusion factor, $(1 - V_2'/V_1') + \Delta(rV_\theta)/2\sigma_m r_m V_1'$

i incidence angle, angle between relative inlet-air direction and tangent to blade mean camber line at leading edge, deg

Δi difference between blade minimum-loss incidence angle and choking incidence angle at Mach 1.0

M Mach number

P total pressure, lb/sq ft

r compressor radius, in.

T total temperature, $^\circ R$

t_{max} maximum blade thickness

V velocity, ft/sec

w weight flow, lb/sec

[redacted]

β air angle, angle between air velocity and axial direction, deg

δ ratio of total pressure to NACA standard sea-level pressure of 2116 lb/sq ft

δ° deviation angle, angle between outlet-air direction and tangent to blade mean camber line at trailing edge, deg

ε cone half-angle, deg

η efficiency

θ ratio of total temperature to NACA standard sea-level temperature of 518.7° R

κ blade angle, angle between tangent to blade mean camber line and axial direction, deg

σ solidity, ratio of chord to spacing

φ blade camber angle, difference between blade angles at leading and trailing edges, $\kappa_1 - \kappa_2$, deg

$\bar{\omega}$ total-pressure-loss coefficient

Subscripts:

ad adiabatic

id ideal

m mean radius (mean mass streamline)

min minimum

t tip

z axial direction

θ tangential direction

0 free stream

1 rotor inlet

2 rotor outlet

Superscript:

' relative to rotor

[redacted]

APPARATUS AND PROCEDURE

The apparatus and procedure used for these tests are described fully in reference 1. A schematic sketch of the test rig showing instrument locations is given in figure 1(a), and the projection of a blade into the radial-axial plane is given in figure 1(b), showing the blade elements for which element data are presented. Also included is a table giving the blade inlet and outlet radii at the intersection with the design elements at 10, 30, 50, 70, and 90 percent of mass.

The important blade-element design parameters for the hub, mean, and tip sections are as follows:

	Hub	Mean	Tip
Flow from outer casing, %	90	50	10
Chord, in.	2.75	2.75	2.75
Solidity, σ	1.963	1.517	1.282
Camber angle, φ, deg	56.36	38.64	28.22
Relative inlet flow angle, β_1', deg	47.38	55.4	62.3
Relative outlet flow angle, β_2', deg	-7.08	17.76	35.08
Design incidence angle, i, deg	5	5	5
Design deviation angle, δ^o, deg	6.9	6	6
Cone half-angle, ε, deg	11.65	3.07	-6.52
Design inlet relative Mach number, M_1'	0.898	1.119	1.258
Maximum thickness, t_{max}, % chord	8.4	6.46	4.9
Design diffusion factor, D	0.48	0.51	0.58

The outer-wall radius was 7.97 inches at the inlet and 7.63 inches at the outlet.

PRESENTATION OF DATA

The over-all performance of the subject rotor is reproduced from reference 1 in figure 2, which gives the usual pressure-ratio and efficiency plots against specific equivalent weight flow in pounds per second per square foot of frontal area. The best over-all performance, which was obtained at 80-percent design speed, indicated a pressure ratio of 1.58 at a rotor adiabatic efficiency of 0.95, corresponding to a spanwise average minimum-loss coefficient of 0.045. For this operating point the absolute rotor-exit velocities (stator inlet) varied from Mach 0.94 at the hub to 0.70 at the tip, as indicated by figure 9(d) of reference 1. Hence, the absolute Mach number at speeds above 80 percent would be well into the critical range. At design speed the best efficiency of 0.87 was obtained at a pressure ratio of 2.03. (The spanwise arithmetic average of the best design-speed minimum losses, which ranged from 0.36 (tip) to 0.063, was 0.15.) For the overspeed point (110-percent design speed) a

peak adiabatic efficiency of 0.81 was obtained at a pressure ratio of 2.24 and a tip relative Mach number of 1.38.

Figure 3, giving the environmental conditions under which the current element data were taken, is also reproduced from reference 1.

The following performance data are presented herein:

	Speed, % design	Figure
Radial-distribution data:		
Inlet and outlet relative Mach numbers, M_1', M_2'	100	3(a)
	80	3(b)
Incidence angle, i	100	4(a)
For best efficiency and minimum loss	100	6(a)
	80	6(b)
Deviation angle, δ°	100	4(b)
Axial velocity ratio, $V_{z,2}/V_{z,1}$	100	4(c)
Diffusion factor, D	100	4(d)
Relative total-pressure-loss coefficient, $\bar{\omega}'$	100	4(e)
Comparison with ref. 4 data	100	5
At minimum-loss incidence angle	100	7
	80	7
Comparison of hot-wire and steady-state data	100	12(a)
	90	12(b)
	80	12(c)
Relative total-pressure recovery, $P_2'/P_{2,id}'$	100	4(f)
Blade-element characteristics:		
Axial velocity ratio, $V_{z,2}/V_{z,1}$		
Relative inlet Mach number, M_1'	110	
Relative total-pressure-loss coefficient, $\bar{\omega}'$	100	8
Diffusion factor, D	80	
Temperature-rise ratio, $\Delta T/T_1$	60	
Deviation angle, δ°		
Adiabatic efficiency, η_{ad}		
Incidence angle, i	110	
	100	8
	80	
	60	
Minimum-loss and choking incidence angles at Mach 1.0 (extension of ref. 2 data)	100	9
	80	
Relative total-pressure recovery (hot-wire data)	100	10(b)
	90	10(c)
	80	10(a)
Typical hot-wire trace		11

[redacted]

DISCUSSION

Radial-Distribution Plots

Rotor operational modes. - The radial-distribution curves (figs. 3 to 7), aside from giving the over-all level of the parameter values, in several instances graphically illustrate the effects on certain parameters of the mode of rotor operation.

The various modes of design-speed operation, which are fully described in reference 1, are designated herein according to the specific equivalent weight flows $w\sqrt{\theta}/\delta A_F$ in pounds per second per square foot:

Maximum flow or minimum back pressure	30.3
Maximum pressure recovery on rotor vertical flow line	30.0
Peak efficiency	29.2
Minimum flow, near surge	27.4

For the runs at 80-percent design speed, which are of interest because of the excellent stage pressure ratio and efficiency accompanying the rather conventional transonic Mach numbers and operational characteristics, the operational modes are defined as follows:

Maximum flow or minimum back pressure	28.1
Peak efficiency	26.6
Minimum flow, near surge	23.4

Inlet and outlet relative Mach numbers. - The order of magnitude of the blade relative diffusion is indicated in figures 3(a) and (b) for 100 and 80 percent of design speed, respectively, by comparison of corresponding values of inlet and outlet relative Mach numbers. Curves are presented on the design-speed figure for each of the operating modes, along with the computed design values of inlet and outlet relative Mach number. For purposes of design comparison the diamond symbols (peak efficiency) should be considered in figure 3. The curves of relative inlet Mach number are similar in shape. The experimental relative outlet Mach number at design speed has roughly the same average level as the design curve, but the distribution is substantially different. Inasmuch as the design distribution was carefully computed considering streamline curvature and the radial variation of enthalpy and entropy, it is important to find the reason for this discrepancy. The much poorer than design tip recovery may be the fundamental cause of the indicated discrepancy in outlet radial distribution.

Incidence and deviation angles. - The manner in which the radial distribution of incidence and deviation angles changes with the operating modes is shown in figures 4(a) and (b) along with the design values. The design incidence was chosen somewhat artibrarily as a good average value based on observation of a large amount of experimental data. The design

deviation angle essentially follows Carter's rule. The small alterations made to the Carter's rule values are negligible. Little can be said about the comparison with the experimental results except that there appear to be strong three-dimensional effects and that the reliability is poor, as it is for all parameters depending on measured outlet static pressures. The incidence-angle agreement could have been somewhat improved through the use of a rule such as those of references 2 or 3, however, had they been available.

4147

Loading parameters. - Two parameters (axial velocity ratio and diffusion factor, figs. 4(c) and (d)) sometimes used to indicate the loading or diffusion level on blade elements are useful in estimating the loss level for a given experimental blade-row loading. The fact that the design and experimental (peak-efficiency distribution, diamond symbols) values do not compare more favorably may be due in part to use of a tip loading that is too high. In reference 4, for example, values of diffusion factor greater than 0.3 at the tip led to an essentially linear increase in losses. Moreover, in order to maintain tip-region efficiencies of 0.90 or above, a tip diffusion factor of 0.45 or lower is indicated. Thus, the design tip section (10-percent mass) loading at design speed for this rotor (D = 0.58) was high enough to cause large losses and alter the design distribution along the entire radius. The diffusion factor and axial velocity ratio are significant only at the minimum-loss incidence angle (most efficient weight-flow point). Therefore, only for the diamond symbols can any correlation with losses be attempted.

The inadequacy of both conventional diffusion factor and axial velocity ratio for predicting losses when the surface Mach numbers are appreciably supersonic is pointed out in reference 5. Some of the following loss analyses further indicate the lack of a unique relation between loss and the more conventional loading parameter D in the Mach number and loading level of interest herein. The dependence of any new and more suitable high-performance loading parameter on peak surface Mach number is indicated in reference 5.

Loss variations. - Two commonly used loss parameters, total-pressure-loss coefficient $\overline{\omega}'$ and rotor blade relative total-pressure recovery, are presented in figures 4(e) and (f). A fair comparison of the losses resulting from a given radial distribution of D (or axial velocity ratio) may be obtained by comparing the diamond symbols of figures 4(c) to (f). The peak-efficiency loss distribution (fig. 4(e)) is fairly close to the minimum-loss distribution, the only conditions for which the loading parameters are significant. A plot of the figure 4(e) losses against the figure 4(d) loading (shown in fig. 5) indicates that the current high-speed losses are all above the loss values indicated for the given D in reference 4. In figure 5, the radial distribution of the loss coefficient for the peak-efficiency design-speed test point is plotted against D computed from the corresponding flow conditions. The

[redacted]

average loss-loading variations for the tip, mean, and hub sections from reference 4 are indicated.

The significant difference between the present tip-section results and the so-called conventional transonic sections for which the diffusion-factor - loss relations were derived lies in the combination of higher inlet relative Mach number (tip design-speed value, 1.258) and loading utilized herein. A simplified two-dimensional analysis indicates that tip-section suction-surface Mach numbers of 1.77 are attained even at the most efficient operating point. Therefore, it appears that, in this Mach number and loading range, loss would not be a single-valued function of D. Observation of the results at 80-percent design speed indicates that the conventional loss and loading correlation previously observed for transonic stages holds true, however. A modified loading parameter giving strong consideration to the maximum suction-surface Mach number may again allow an essentially single-valued relation between loading and loss.

The peak suction-surface Mach number for the assumed most-efficient flow configuration about a family of double-circular-arc blades (nearly attached bow wave followed by subsonic flow in the blade passage, similar to fig. 10 of ref. 5) depends on the blade geometry (blade angle κ, camber angle φ, solidity σ, and maximum thickness t_{max}). Therefore, these parameters may possibly be eliminated from an approximate relation between loss and peak surface Mach number. If this is possible, a particularly useful and simple general relation should result, from which other useful optimization may be made. For example, with other parameters fixed, the solidity effect on local suction-surface Mach number and hence losses might be ascertained. A qualitative discussion of this effect appears in reference 5. From such considerations the hub solidities, which are usually too high, might be optimized within the structural requirements and the minimum allowable tip solidity (min. before catastrophic loss rise). A collection of the available experimental loss and surface Mach number data is required, however, before the existence and uniqueness of such a relation can be established.

Incidence-angle variations. - The design and experimental radial distributions of incidence angle (fig. 6(a)) do not agree particularly well. There is, however, only a small difference between the measured incidence angle at the design peak-efficiency test condition and the section minimum-loss incidence. This agreement is probably fortuitous, however. Actually, the experimental incidence-angle curve for the peak-efficiency test point varies in the same manner with radius as the curve representing the experimental optimum section incidences rather than in the manner of the assumed design incidence-angle distribution. The curves for 80-percent design speed (fig. 6(b)) do not agree quite as well.

These curves indicate the inability to operate all blade elements simultaneously at minimum-loss incidence. In view of these curves, however, the corresponding radial variations of loss coefficients given in

figure 7 are good indications of the best (lowest) loss coefficients attainable by this rotor under these operating conditions. There is a marked increase in losses as speed is increased from 80 to 100 percent of design speed. The curves of radial loss variation for both 100- and 80-percent design speed show rapidly rising loss coefficients toward the inner and outer walls, where the wall viscous effects are present. In addition to the wall viscous effects, the tip region suffers from the previously mentioned high tip loading and the tip-clearance core loss mentioned in reference 6, discussed more fully in reference 7, and further discussed later in this report.

Blade-Element Data (Steady-State Instrumentation)

General considerations. - The blade-element data plotted in figure 8 against incidence angle are presented in the usual manner. The element performance parameters (loss coefficient $\bar{\omega}'$, deviation angle δ°, adiabatic efficiency η_{ad}, temperature-rise ratio $\Delta T/T_1$, axial velocity ratio $V_{z,2}/V_{z,1}$, and diffusion factor D) and the Mach number M_1' and incidence angles i at which they are obtained probably constitute the most useful and informative data available to the designer.

In general, the curves are self explanatory; however, a few general and specific observations will be made regarding them. First, all the parameters that depend either directly or indirectly on rotor-outlet static-pressure measurements (δ°, $V_{z,2}/V_{z,1}$, and D) show considerable scatter because of the difficulty in accurately measuring static pressure with the current outlet configuration and Mach numbers. The other parameters ($\bar{\omega}'$, M_1', $\Delta T/T_1$, and element efficiency η_{ad}) are both consistent and generally conventional in trend.

Element loss factor and adiabatic efficiency. - The loss-coefficient and efficiency curves at each element and speed show rather distinct optimum points, indicating that the rotor was tested essentially over its entire useful performance range. The weight-flow variation was rather large at all speeds, the curves for 80, 90, 100, and 110 percent of design speed having ranges of approximately 20, 15, 10, and 10 percent of the maximum flow rate, respectively. For a given speed, the minimum loss and the minimum incidence angle gradually move to higher incidences with decreasing radius, as might generally be expected from blade thickness and solidity considerations (refs. 3 and 8). The arithmetic average of the element adiabatic efficiencies is 0.873 for the best design-speed point.

The design-speed loss level never drops below 0.10 at any element. The element efficiencies still reach peak values of the order of 0.95 at some elements, however, giving some indication that reasonably high loading may be desirable when blade inlet relative Mach numbers are high (see figs. 24 and 25 of ref. 3). This statement implies that, with respect to efficiency, an optimum work input exists for each value of inlet relative

Mach number. However, any valid optimization should be made from more elaborate stage considerations, including the stator-inlet flow effects on stator losses.

At 100 and 110 percent of design speed, where the combination of inlet Mach number and loading (and, therefore, surface Mach number) is highest (but probably not the optimum combination), the tip losses ($\omega\zeta$ = 0.43 at 110-percent speed) clearly impair the over-all performance. The specific cause of the poor tip flow is not certain. It may be possible, however, to improve over-all performance at this level by unloading the tip in order to reduce or compensate for other tip flow complications such as tip-clearance effects.

At or below 80-percent design speed, losses are low over a broad range, even though the work level remains reasonably high. With regard to both efficiency and operating range, this would appear to be an excellent Mach number and loading range in which to design high-performance rotors.

Work input, deviation angle, and axial velocity ratio. - In spite of the scatter of the deviation-angle data points, there is an apparently consistent decrease in deviation angle with decreasing incidence angle for each element and speed at the lowest incidence angles (lowest back pressure). This behavior, which is contrary to much of that indicated by other rotors (e.g., refs. 5 and 9), may be explained as follows: When the outlet relative Mach number is sonic or supersonic, the static pressure at the blade outlet may be sufficiently lower than the static pressure between blades to necessitate blade trailing-edge expansions. In order to satisfy continuity, then, the flow deflection must be more toward the axis for the low static pressure than for the higher outlet static pressure. At all except the hub element, such deflection results in decreased deviation. For these tests this phenomenon is as closely related to the test rig and laboratory exhaust system as to the rotor, however.

This decrease in deviation is accompanied by either a constant enthalpy or slight decrease in enthalpy, as indicated by the curves of temperature-rise ratio. Inasmuch as the incidence-angle change is generally smaller than the deviation change, it appears that a net increase in relative turning results in either no change or a small net decrease in work. In order to explain this apparent paradox, the axial velocity ratio must be considered. The extremely large increase in this term at the lowered incidence angles (fig. 8) changes the velocity diagram in such a manner that the net enthalpy rise as represented by ΔV_θ is reduced. Fundamentally, the blade surface velocities change in such a manner that the net circulation is reduced at the lowered incidences (i.e., lowered back pressures). The fact that both the outlet blade and relative flow angles (κ_2 and β_2') are relatively close to zero (near axial, see table on p. 4) along the entire blade span is also a significant factor in the near constancy of the element work coefficient.

The increased losses result from the eventual shock necessitated by the supersonic expansion. In general, the effects of deviation angle and axial velocity ratio are almost exactly complementary, as indicated by the enthalpy rise (temperature-rise ratio) below the tip element.

The fairly general increase in deviation angle on the high-incidence-angle side (high back pressure) is due to the normal viscous effects with increased back pressure, as is commonly noted in other experimental investigations.

4147

CX-2 back

Inlet relative Mach number and diffusion factor. - The inlet relative Mach number is presented for the purpose of providing that information to the reader at each incidence angle. The diffusion factor, as previously mentioned, is susceptible to measurement errors; however, the expected general trends still exist in its variation. The dominating term in the diffusion-factor expression is the relative velocity ratio V_2'/V_1', which at low incidence angles leads to very low and meaningless values of D. Actually, the only significant diffusion factors on these curves are those values at the minimum-loss incidence angle for each element and speed. In addition, while the tip values of D may be significant in some respect, they do not conform to the relations of diffusion factor and loss presented in the original paper on the subject (ref. 4). This condition is probably due to the previously mentioned high peak suction-surface Mach number and other secondary-flow effects. Also, as stated in reference 1, the tip design diffusion factor (D = 0.58) is probably above the prudent level.

Minimum-loss and choking incidence angles at Mach 1.0. - The element minimum-loss coefficient and the incidence angle at which this loss occurs were tabulated for several radial blade elements of the current rotor. The choking incidence angle at an inlet relative Mach number of 1.0 was then found from the procedure of reference 2. The difference between the Mach 1.0 choking incidence angle and the minimum-loss incidence angle Δi was then plotted against inlet relative Mach number. Since the results from the current rotor tests agreed rather well in the low Mach number range with those of reference 2, the curves of Δi against M_1' from that report are reproduced in figure 9 with both the low Mach number corroborating points and the higher Mach number extension points added. Curves are presented for the hub, mean, and tip regions. The original experimental data were compiled from several rotors and a cascade. They appear to offer a satisfactory criterion for setting double-circular-arc design incidence angles. The present report is specifically concerned with the effect of increased inlet relative Mach number and loading (which affects surface Mach number) on the parameter Δi. Theoretically, as relative inlet Mach number increases, above some critical supersonic value the difference Δi must begin to decrease with Mach number. There is inconclusive evidence that there actually is a drop in Δi above M_1' values of 1.2 (fig. 9(c)). In general, the correlation suggested in reference 2 still appears to be valid from the current results.

[redacted]

Element Blade-to-Blade Loss Variation (Hot-Wire Measurements)

General considerations and typical subsonic trace. - For analytical purposes, the approximate blade-to-blade variation of the rotor blade relative total-pressure recovery $P'_2/P'_{2,id}$ is presented in figure 10. The relative total-pressure recovery is plotted against the distance from the suction surface of the blade as a percentage of the total tangential blade spacing. The equipment, measuring technique, and data-reduction procedure used are described in reference 6.

With the very small wires required in order to get a sufficiently high frequency response from the hot-wire anemometer, extreme difficulty was experienced in obtaining measurements at the rotor tip before the wire failed. For this reason, the data presented do not always provide the ideal illustration desired. However, these data do cover a sufficiently wide range of test conditions to allow identification of several separate loss phenomena. For later comparison with the hot-wire anemometer results, a typical subsonic wake survey is presented in figure 11.

The tangential distributions of element losses presented in figure 10 are approximate, primarily as the result of the data-reduction procedure, the limitations of which are described in reference 6. These curves indicate graphically fundamental changes in the source of the losses as speed, and hence inlet relative Mach number and loading, is changed.

In order to facilitate the discussion of the hot-wire recovery traces, a typical subsonic blade loss profile wherein no separation, secondary flow, or other flow complications exist is shown in figure 11. Here the entire measurable total-pressure defect arises from viscous wall shear on the blade and is concentrated in the wake. The static pressure is assumed constant in the tangential direction, and the minimum velocity in the wake just at the blade trailing edge is approximately zero. Surveys farther downstream would indicate a broadening wake and increasing minimum velocity as the wake flow is reenergized through shear at the expense of the free-stream pressure energy.

Reference 10, which treats the wake flow processes for incompressible flow, shows that the wake is reenergized very rapidly immediately behind the trailing edge. For low-speed flow, the minimum wake velocity rises from zero at the trailing edge to 80 percent of the free-stream value 0.15 to 0.40 chord length downstream, while the boundary-layer form factor changes by a corresponding magnitude. Hence, most of the total-pressure mixing losses, which depend on the boundary-layer momentum thickness and form factor, occur in this interval. For low-speed flow, both the momentum thickness and the form factor are then empirically related to the chord-length distance downstream. Unfortunately, no such

relations or data from which such relations might be reliably deduced are currently available for compressible flow. For this reason, it is difficult to say with certainty which of the traces in figure 10, based on measurements taken approximately 0.30 chord length downstream, indicate separated flow. Despite the inconclusiveness of the data in this sense, a qualitative picture of the flow sequences is indicated.

At least three loss sources different from that of the typical subsonic element variation just described are indicated in figure 10:

(1) Blade suction-surface shock losses

(2) Separation and attendant mixing losses

(3) Tip core losses

Among other things, these losses depend on the inlet relative Mach number and the blade loading (camber), the precise parameters whose effects it was desired to investigate.

Peak efficiency at 80-percent design speed. - The tangential loss distributions for elements on the 10-, 20-, 40-, 60-, 80-, and 90-percent-mass streamlines for a test point at 80-percent design speed near peak efficiency (rotor $\eta_{ad} \approx 0.95$) are shown in figure 10(a). The traces between the 40- and 90-percent mass sections resemble closely the conventional subsonic element wake survey, except for the width of the wake. At these sections and speed, the element inlet relative Mach number is just approaching the level where the maximum surface Mach numbers become appreciably supersonic and the flow characteristics begin to change. For computational purposes, a constant reference pressure recovery of 1.0 is indicated over some 60 percent of the blade passage circumferentially. These computations, which neglect inlet losses and assume that the highest recovery corresponds to a no-loss region, are probably reasonably accurate in the transonic region, as is indicated by figure 12. At somewhat higher Mach numbers, where the free stream experiences higher shock losses, serious errors in absolute losses would result from this assumption. The extra wide yet distinct wake at 80-percent mass suggests that mild shocks may occur near the surface, adding to the normal boundary-layer momentum defect and extending a short distance into the free stream.

The innermost section (90-percent mass) shows the wake effect extending over 65 percent of the passage width despite the lower inlet relative Mach number at this radius. However, since the magnitude of the defect is probably not large enough to indicate separation at this position (0.30 chord length behind the rotor trailing edge), the most plausible reason for this loss spread is the effect of hub wall boundary layer and secondary flow.

The tip section (10-percent mass) indicates a broad wake and a momentum defect extending over 80 percent of the passage width. The greater portion of this defect is restricted to approximately 30 percent of the passage, however. Some suction-surface shock effects are certainly present in this region (inlet relative Mach number, approximately 1.02), along with some tip-clearance and secondary-flow effects. Here again the relatively wide wake implies shock-magnified viscous losses on the blade suction surface.

Design-speed low-back-pressure surveys. - The design-speed point for which the surveys (fig. 10(b)) were taken was essentially at open throttle; hence, only very limited significance can be attached to the results. As indicated in reference 1, the blade passage area sequence will not allow supersonic flow from hub to tip throughout the rotor and still satisfy even the lowest downstream static pressure. Thus, somewhat in the manner of an overexpanded supersonic nozzle but considerably more complex, a shock of appreciable strength occurs inside the blade passage, causing large losses and probably reaccelerating to the point required to satisfy the downstream boundary condition. This shock accounts directly for a substantial portion of the very large losses indicated in figure 10(b) and indirectly for much of the remainder due to separation. The total-pressure recoveries drop as low as 0.43 for the 10-percent-mass section near the tip. In addition, these recoveries are computed on the assumption that a free-stream region of 100-percent recovery exists. Since no region exists where the actual recovery reaches quite to 1.0, the level of the recovery factors of figure 10(b) is probably too high by an indeterminate amount.

Loss cores. - Three types of blade-row losses (normal wake, separated-flow wake, and shock) have been illustrated in the preceding descriptions. A fourth related type of loss is next illustrated by the tip traces for 90-percent design speed (fig. 10(c)). Here what appears to be a second wake appears just to the right of the passage centerline. This second loss region is actually larger than the conventional wake. This region, located always near the tip, is described in reference 6 as a tip loss core. Analysis of hot-wire measurements indicated that this low-momentum core was in addition to and essentially independent of the normal wake-momentum defect. The low-momentum core is just barely detectable at the 20-percent-mass radius.

The source of the core loss in incompressible fluids is investigated both theoretically and experimentally in reference 7. The core is shown to result from a blade tip vortex sheet that quickly rolls up from the tip-clearance flow and trails downstream of the tip trailing edge. The poor tip efficiency that has frequently been observed for highly loaded transonic stages apparently results at least in part from the movement of the tip-clearance vortex into the free-stream region near the tip to form a core or vortex of lower than free-stream recoverable pressure energy.

[redacted]

Comparison of Steady-State and Hot-Wire Measurements

In order to illustrate the reliability of the hot-wire measurements presented in figure 10, the radial distribution of loss coefficient computed from both the hot-wire and steady-state instrument measurements is presented in figure 12. The tailed symbols represent values computed from steady-state instrumentation, while the plain symbols represent values obtained from integration of the hot-wire measured momentum defects. Identical symbols except for the tail should be compared. The agreement is in general surprisingly good, particularly at the low-loss points. Only the open-throttle 80-percent-speed point shows significant deviation. The hot-wire measurements can therefore be regarded as at least good qualitative indications of the circumferential loss distribution. The conclusions drawn from these data therefore appear valid.

4147

CONCLUDING REMARKS

The present results indicate that the simple element design procedure might be used successfully up to the Mach number and loading level at 80-percent design speed. In order to obtain satisfactory results near design speed, the following suggestions are offered:

(1) Additional loss data should be obtained at higher Mach numbers and loadings as functions of a new and more appropriate loading parameter considering such factors as maximum surface Mach number.

(2) Additional deviation-angle data in the region of these surface Mach numbers should be obtained in order either to substantiate the currently used deviation-angle rules (e.g., Carter's rule) or to provide a new rule.

(3) At the higher inlet relative Mach number levels the theoretical choking incidence angle should be computed and empirically related to either the experimental choking or minimum-loss incidence angles in order to ensure ample operating range.

(4) Finally, a procedure should be used for quantitatively evaluating and allowing for the tip core and other three-dimensional losses in order to prevent three-dimensional choking of the blade passage. This allowance could take the form of an extra blockage allowance at the cascade exit (in addition to that resulting from assumed element losses).

SUMMARY OF RESULTS

Blade-element data for a transonic axial-flow-compressor rotor with double-circular-arc blades, designed on the basis of conventional blade-element principles, were analyzed. The rotor was run up to an overspeed

(110-percent design) tip relative Mach number of 1.38 with a work level corresponding to a pressure ratio exceeding 2.2. The following results were obtained:

1. The best over-all performance, which was comparable to the best transonic-rotor performance thus far presented, was obtained at 80 percent of the design (1260 ft/sec) tip speed. At this point the element work and loss level resulted in an over-all rotor pressure ratio of 1.58 at an adiabatic efficiency just over 0.95. Curves of loss against incidence angle indicate a wide range of low losses and a spanwise average minimum loss of approximately 0.045. Tip relative Mach number was 1.02. Absolute rotor-exit velocities (stator inlet) varied from 0.94 at the hub to 0.70 at the tip. 4147

2. The spanwise arithmetic average of the best design-speed minimum losses, which ranged from 0.36 (tip) to 0.063, was 0.15. Because of the high work level, the arithmetic average of the corresponding element adiabatic efficiencies was still 0.873, leading to an over-all rotor pressure ratio and efficiency of 2.03 and 0.87, respectively.

3. Hot-wire measurements taken about 1/3 chord length downstream of the blade trailing edges allowed an approximate blade-to-blade determination of the blade relative total-pressure recovery. From these hot-wire results the losses were qualitatively attributed to the following sources:

(a) Normal viscous boundary-layer momentum sources

(b) Suction-surface shock losses

(c) Tip-clearance core losses

(d) Separation and secondary-flow losses at both the inner and outer walls

4. Rotor blade-row loss was not a unique function of conventional diffusion-factor loading parameter for the current design-speed combination of loading and inlet relative Mach number.

5. Peak blade surface Mach numbers, which depend on both inlet relative Mach number and blade camber, are indicated as an important loss criterion.

6. Previously presented curves relating minimum-loss incidence to choking incidence at Mach 1.0 as a function of inlet relative Mach number were extended to higher inlet relative Mach numbers with data from the current tests.

[redacted]

7. Overspeed element performance indicates a rapid acceleration of the performance deterioration that began at 90-percent design speed leading to a tip minimum-loss coefficient of 0.43 at 110-percent design speed. Best 110-percent-speed over-all performance showed a rotor adiabatic efficiency of 0.81 and a pressure ratio of 2.24.

8. The general level of the velocity ratios was such that at all speeds above 80-percent design the stator-inlet Mach numbers at the rotor minimum-loss point would be in the critical Mach number region where stator losses have been observed to be high.

9. The weight-flow range was rather wide at all speeds, the curves for 80, 90, 100, and 110 percent of design speed having ranges of approximately 20, 15, 10, and 10 percent of the maximum flow rate, respectively. All of the element data indicated a minimum loss at one incidence angle with increasing loss on either side, giving evidence that this rotor was tested over its entire useful range.

Lewis Flight Propulsion Laboratory
National Advisory Committee for Aeronautics
Cleveland, Ohio, July 10, 1956

REFERENCES

1. Wilcox, Ward W., and Wright, Linwood C.: Investigation of Two-Stage Counterrotating Compressor. I - Design and Over-All Performance of Transonic First Compressor Stage. NACA RM E56C15, 1956.

2. Wright, Linwood C., and Schwind, Richard: Throat-Area Determination for a Cascade of Double-Circular-Arc Blades. NACA RM E55H25a, 1955.

3. Robbins, William H., Jackson, Robert J., and Lieblein, Seymour: Blade-Element Flow in Annular Cascades. Ch. VII of Aerodynamic Design of Axial-Flow Compressors, vol. II, pp. 97-156. NACA RM E56B03a, 1956.

4. Lieblein, Seymour, Schwenk, Francis C., and Broderick, Robert L.: Diffusion Factor for Estimating Losses and Limiting Blade Loadings in Axial-Flow-Compressor Blade Elements. NACA RM E53D01, 1953.

5. Schwenk, Francis C., and Lewis, George W., Jr.: Experimental Investigation of a Transonic Axial-Flow-Compressor Rotor with Double-Circular-Arc Airfoil Blade Sections. III - Comparison of Blade-Element Performance with Three Levels of Solidity. NACA RM E55F01, 1955.

6. Fessler, Theodore E., and Hartmann, Melvin J.: Preliminary Survey of Compressor Rotor-Blade Wakes and Other Flow Phenomena with a Hot-Wire Anemometer. NACA RM E56A13, 1956.

7. Rains, Dean A.: Tip Clearance Flows in Axial Flow Compressors and Pumps. Rep. No. 5, Hydrodynamics and Mechanical Eng. Labs., C.I.T., June 1954. (Navy Contract N6-ori-102, Task Order IV and Nord 9612.)

8. Lieblein, Seymour: Review of High-Performance Axial-Flow-Compressor Blade-Element Theory. NACA RM E53L22, 1954.

9. Creagh, John W. R.: Performance Characteristics of an Axial-Flow Transonic Compressor Operating up to Tip Relative Inlet Mach Number of 1.34. NACA RM E56D27, 1956.

10. Lieblein, Seymour, and Roudebush, William H.: Low-Speed Wake Characteristics of Two-Dimensional Cascade and Isolated Airfoil Sections. NACA TN 3771.

[redacted]

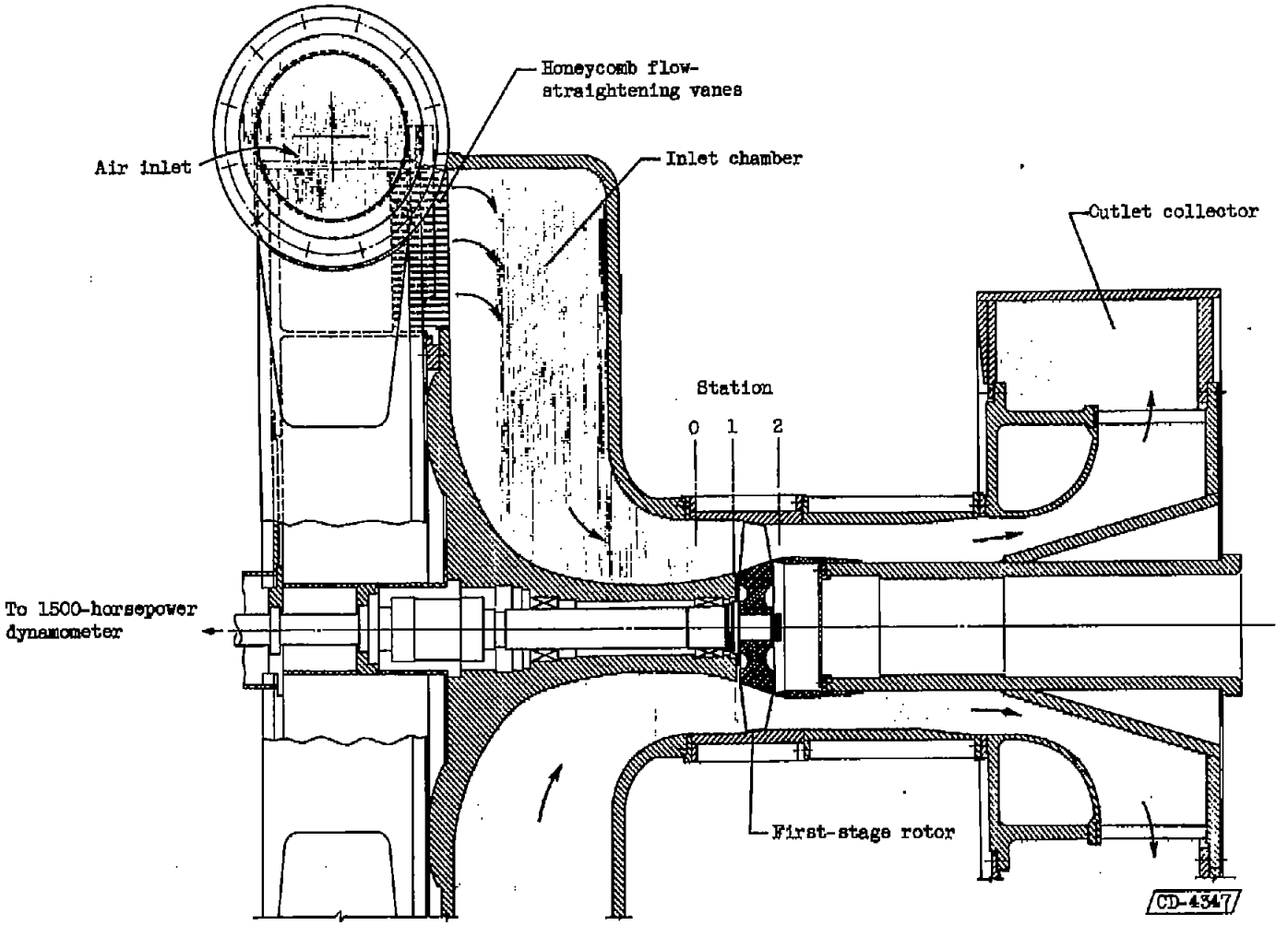

(a) Section through test rig.

Figure 1. - Radial-axial-plane section of rotor and test rig.

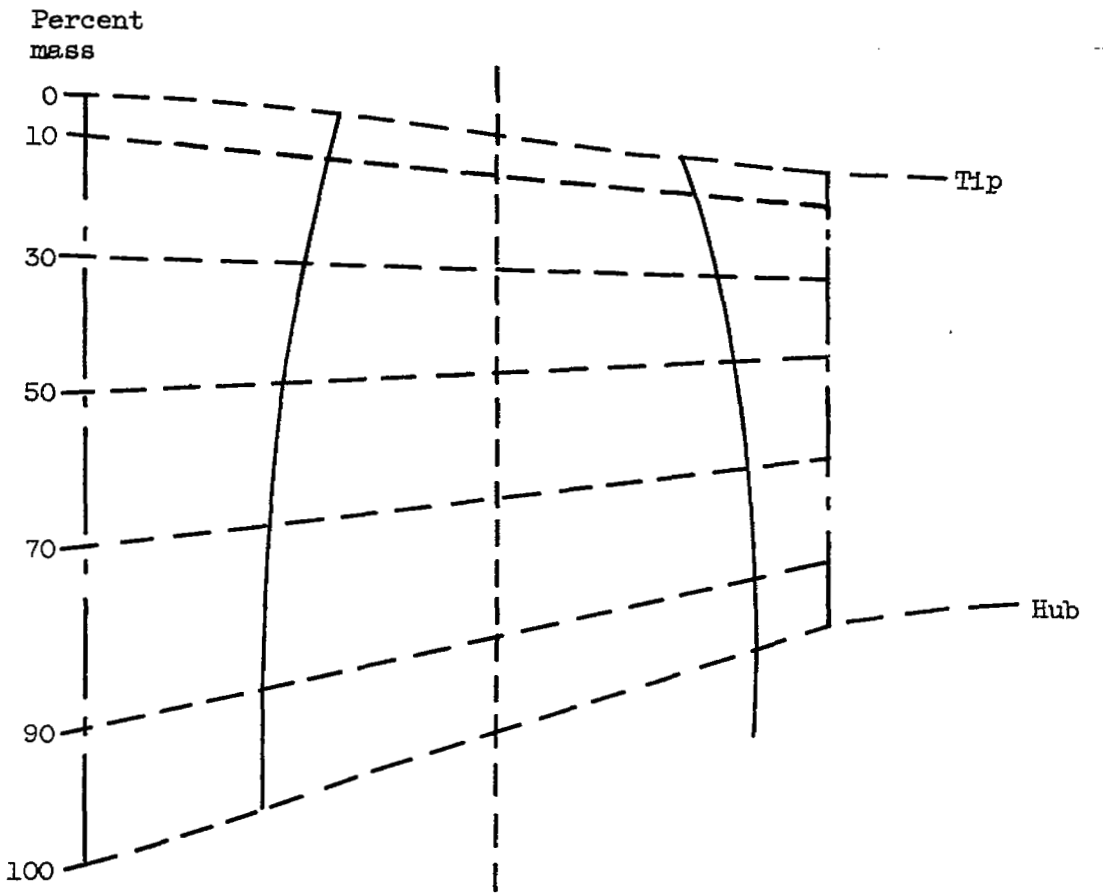

Percent mass	Inlet radius, in.	Outlet radius, in.
10 (tip)	7.65	7.36
30	7.00	6.92
50	6.32	6.45
70	5.53	5.90
90 (hub)	4.53	5.27

(b) Blade projection in radial-axial plane and design stream surface dimensions.

Figure 1. - Concluded. Radial-axial-plane section of rotor and test rig.

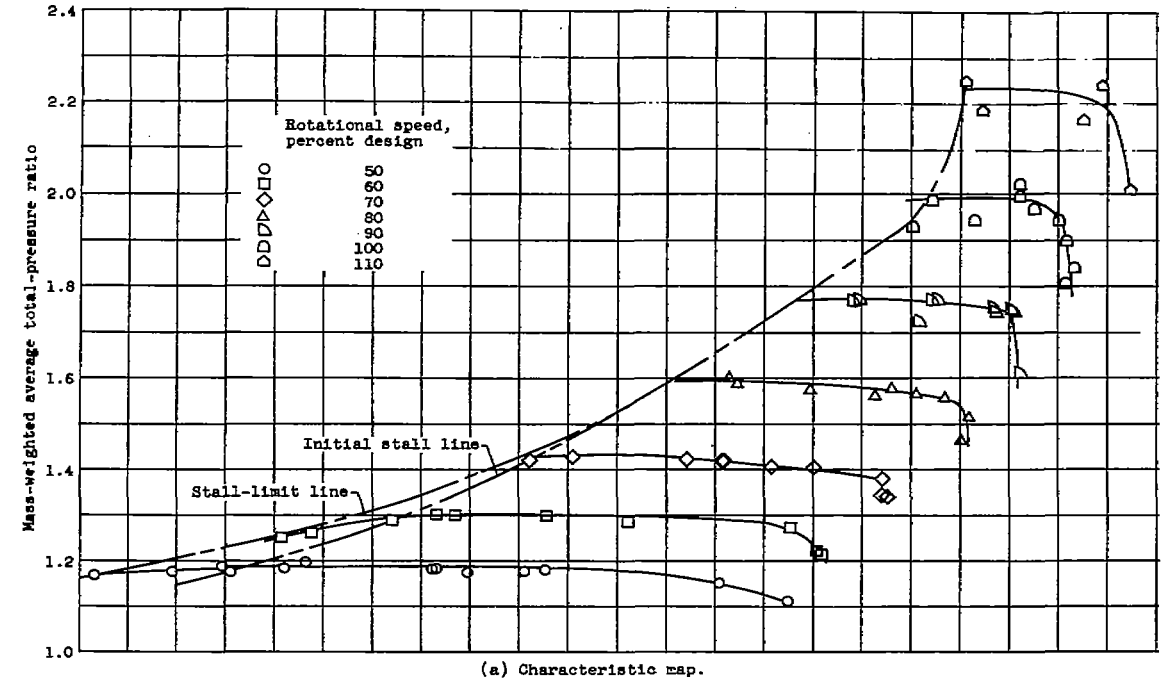

(a) Characteristic map.

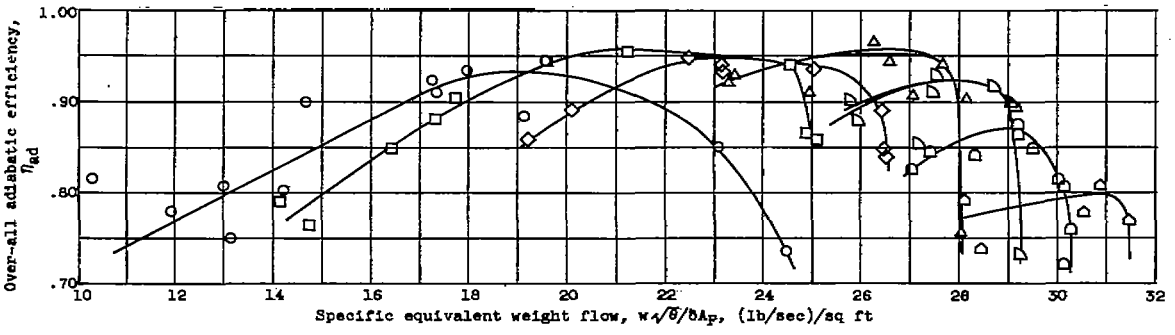

(b) Adiabatic efficiency.

Figure 2. - Over-all performance of first-stage rotor of counterrotating compressor (ref. 1).

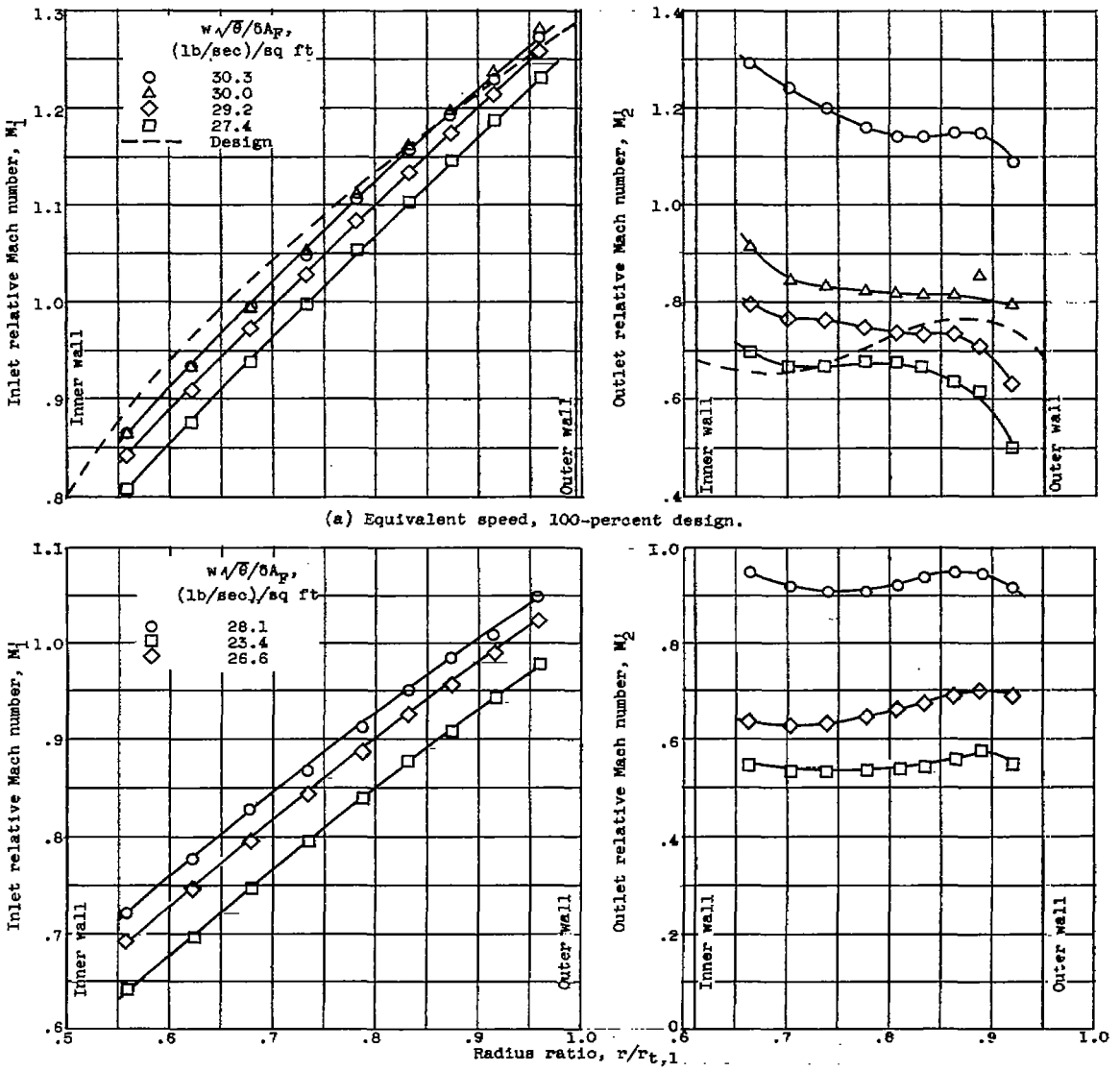

(a) Equivalent speed, 100-percent design.

(b) Equivalent speed, 80-percent design.

Figure 3. - Radial variation of relative Mach numbers for first-stage rotor of counterrotating compressor (ref. 1).

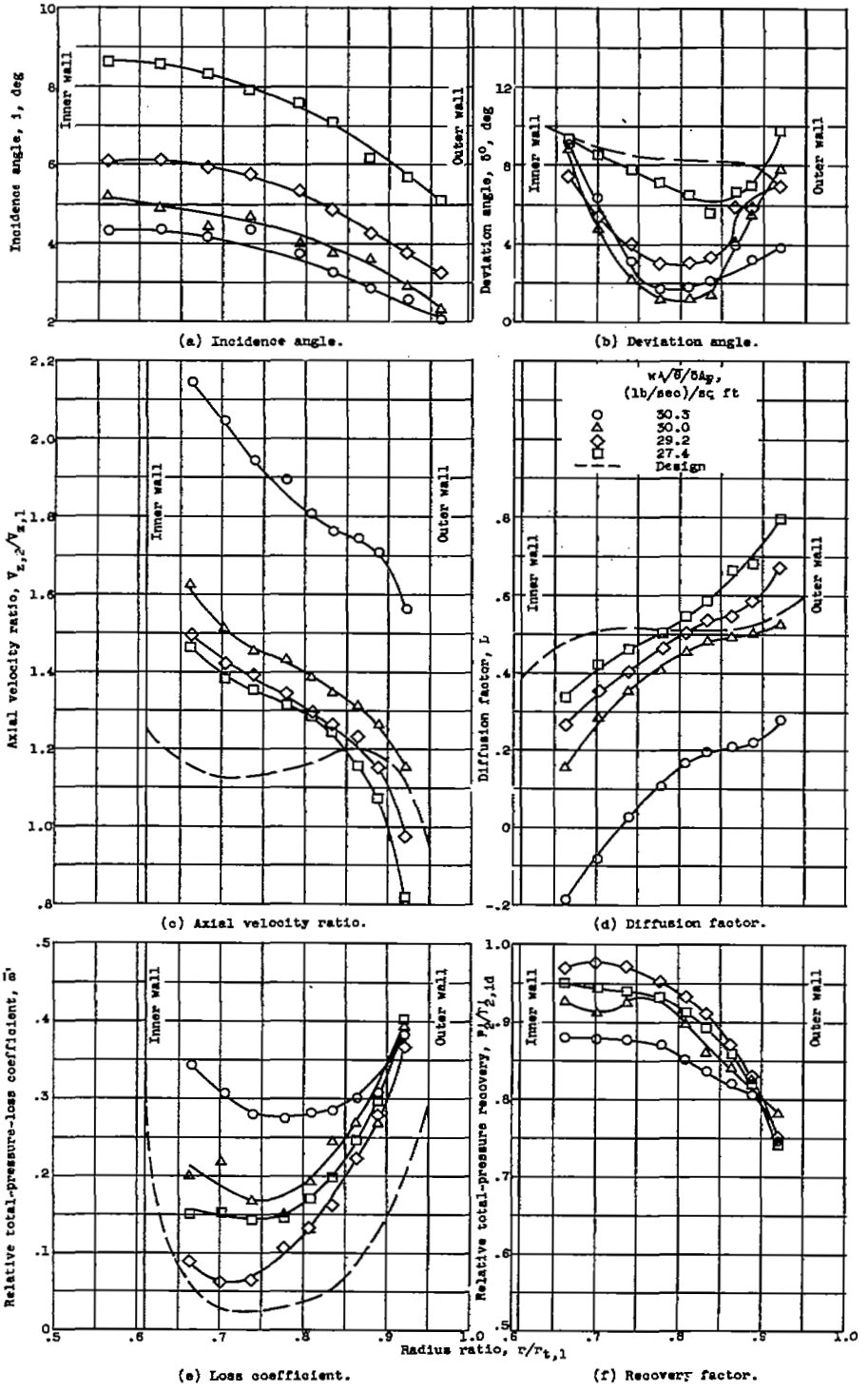

Figure 4. - Radial variation of incidence and deviation angles and loading and loss parameters at design speed.

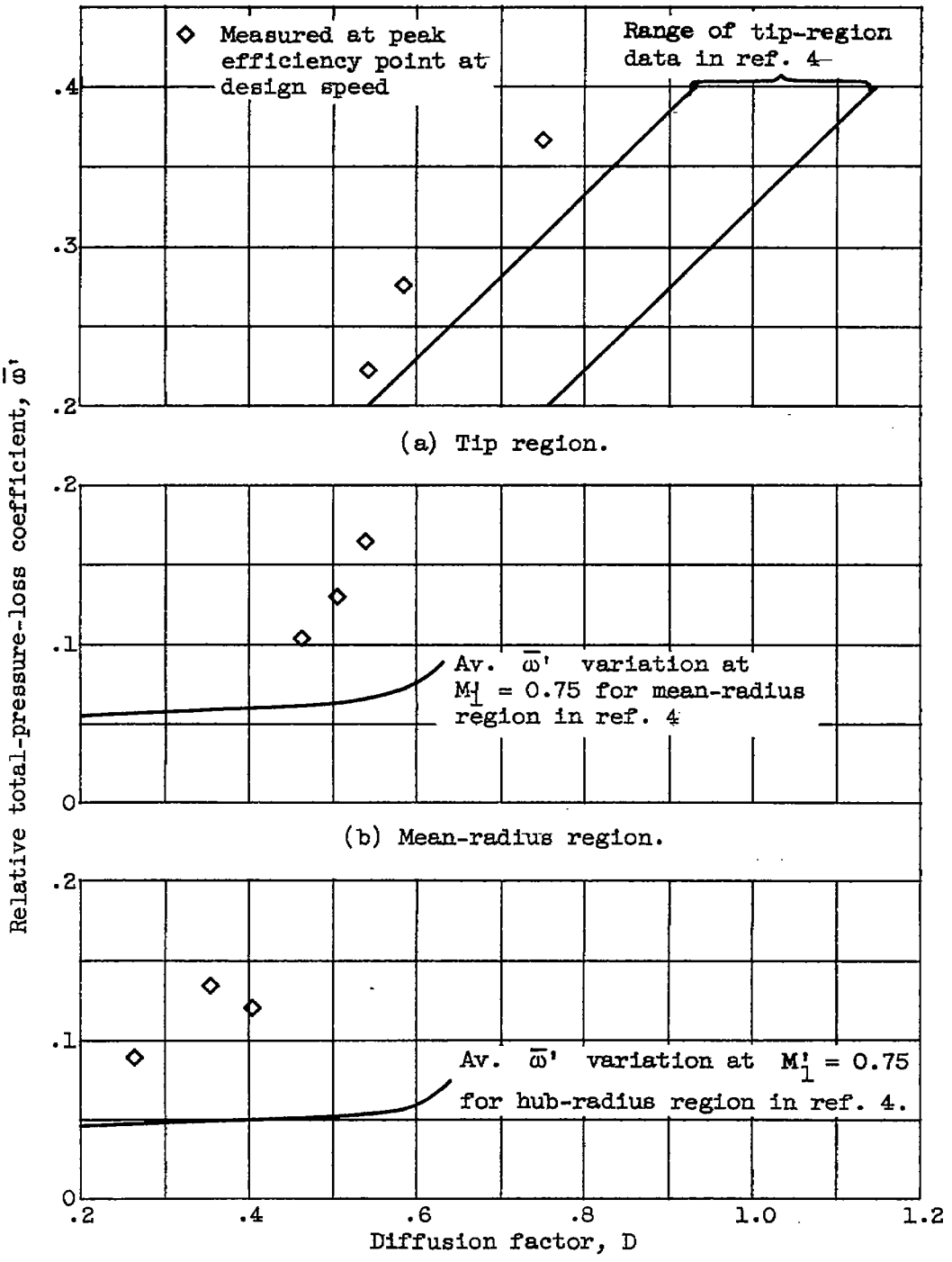

Figure 5. - Comparison of loss-coefficient - diffusion-factor variation with average variation in conventional transonic rotor.

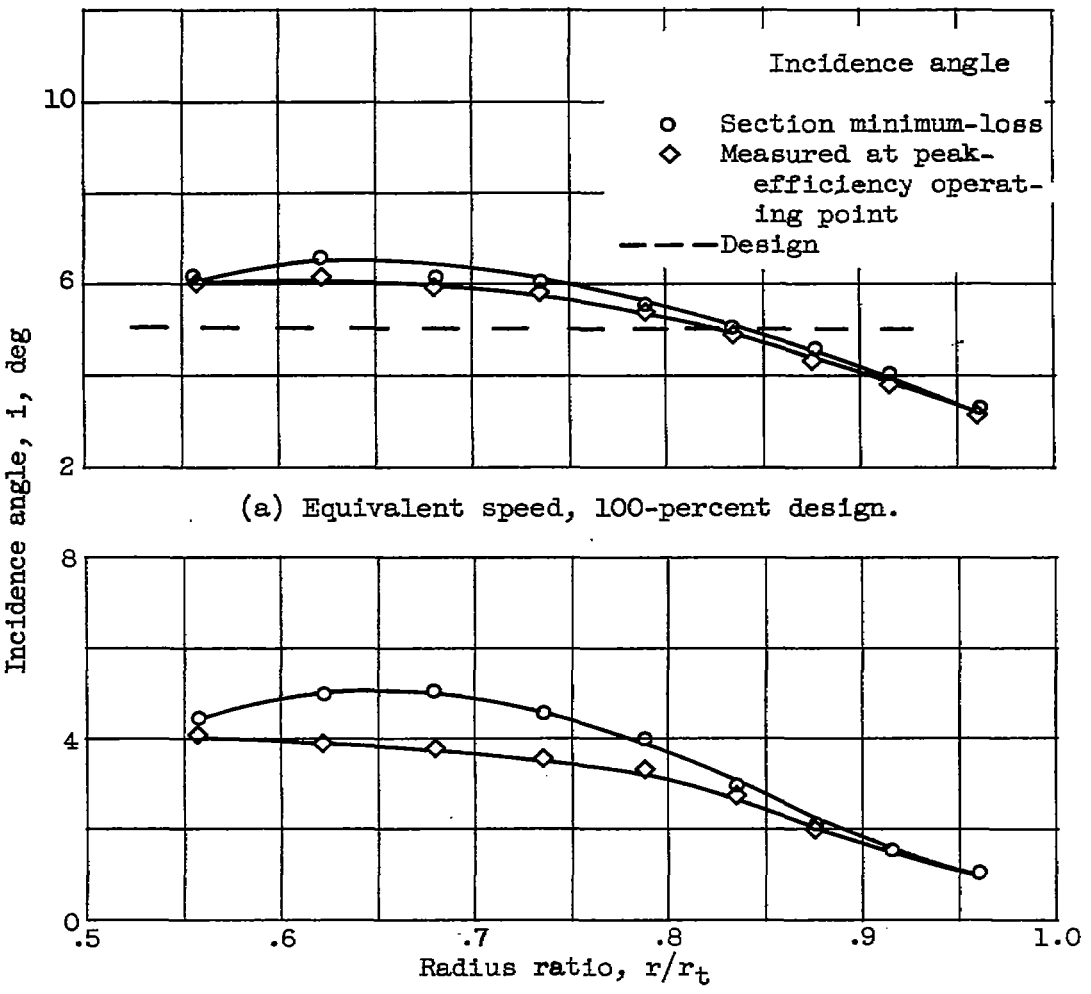

(a) Equivalent speed, 100-percent design.

(b) Equivalent speed, 80-percent design.

Figure 6. - Radial variation of incidence angles for best efficiency and section minimum loss.

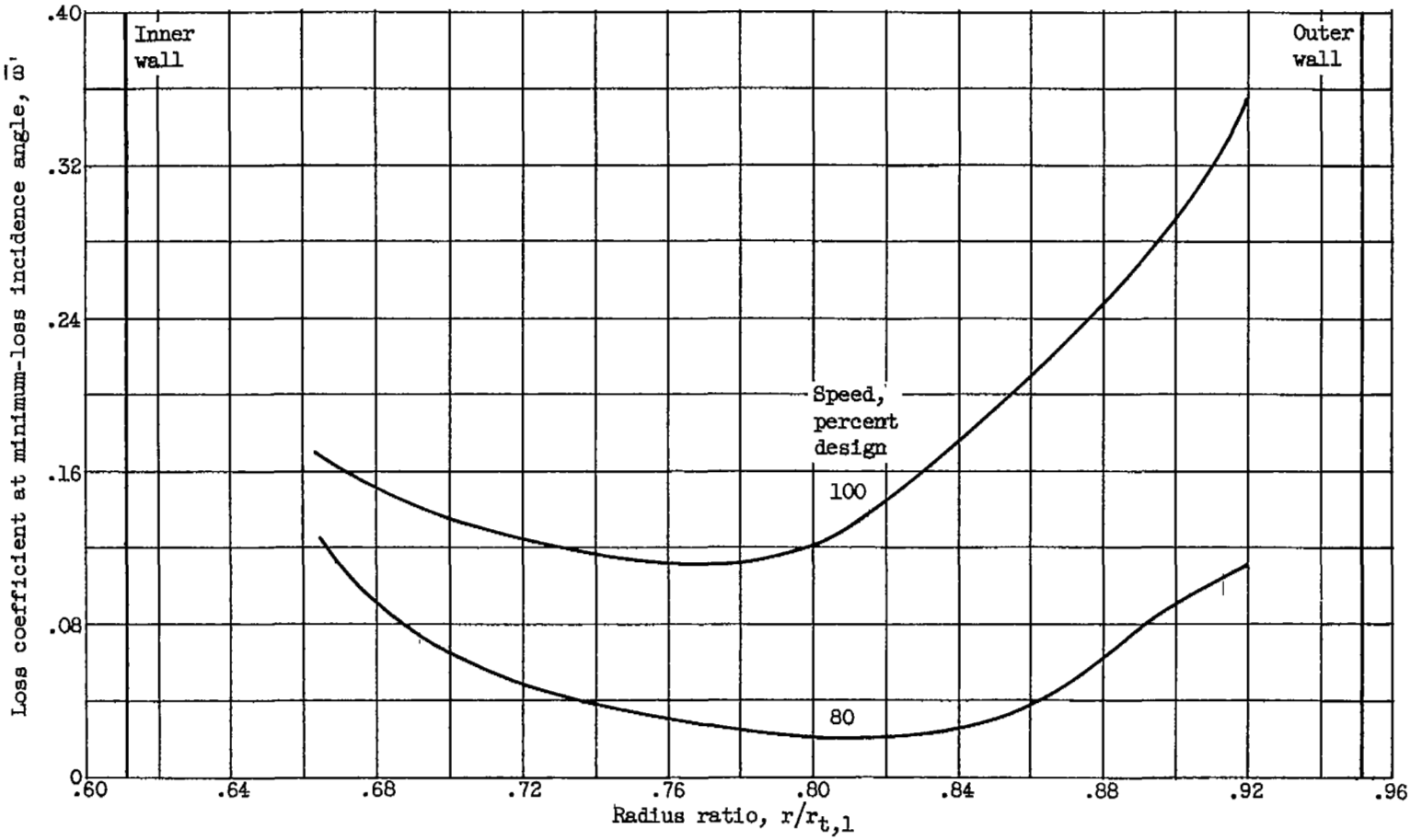

Figure 7. - Radial variation of blade loss coefficient at minimum-loss incidence angle.

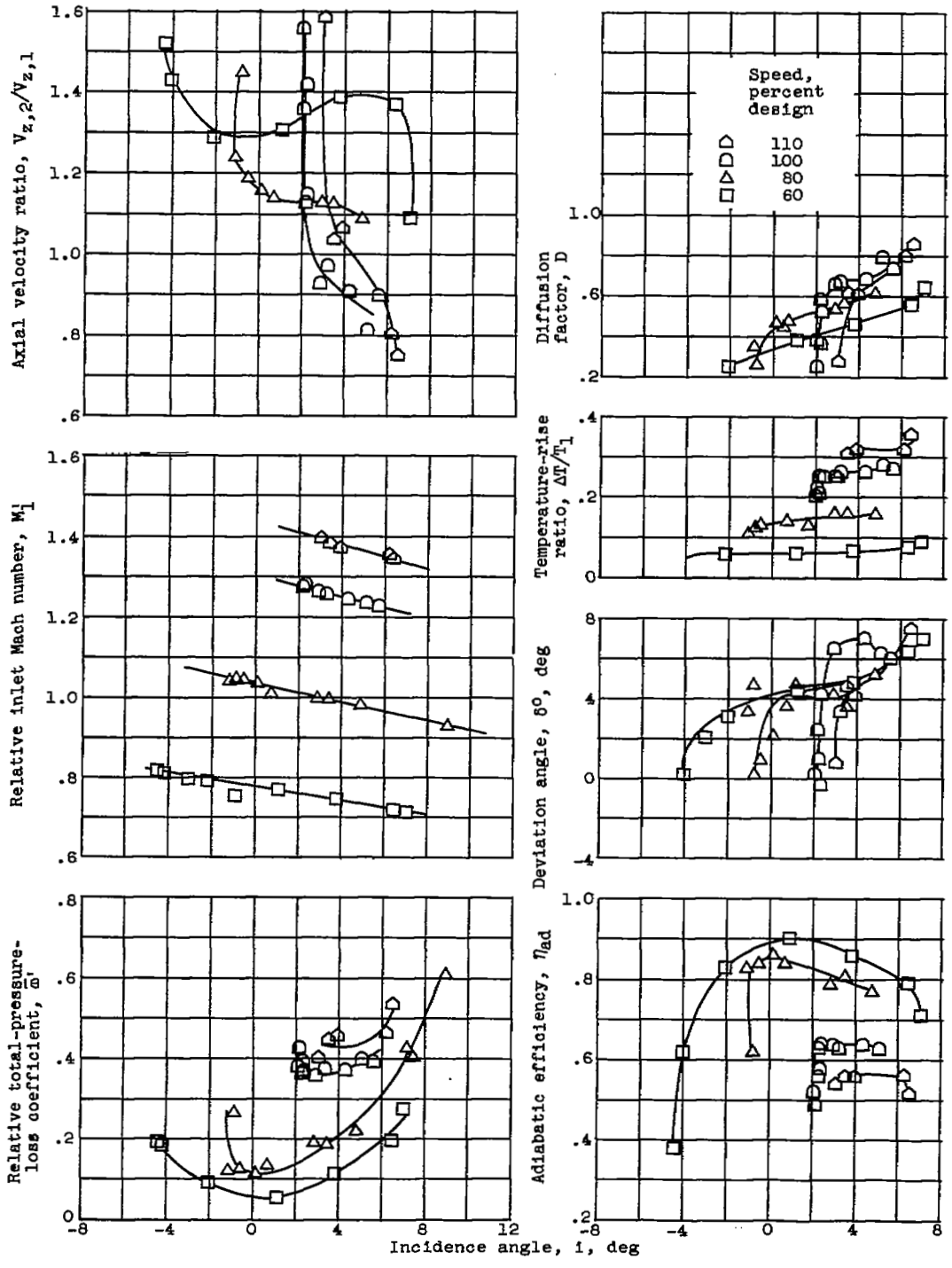

(a) 10-Percent-mass element; r_1 = 7.65 inches, r_2 = 7.36 inches.

Figure 8. - Blade-element characteristics.

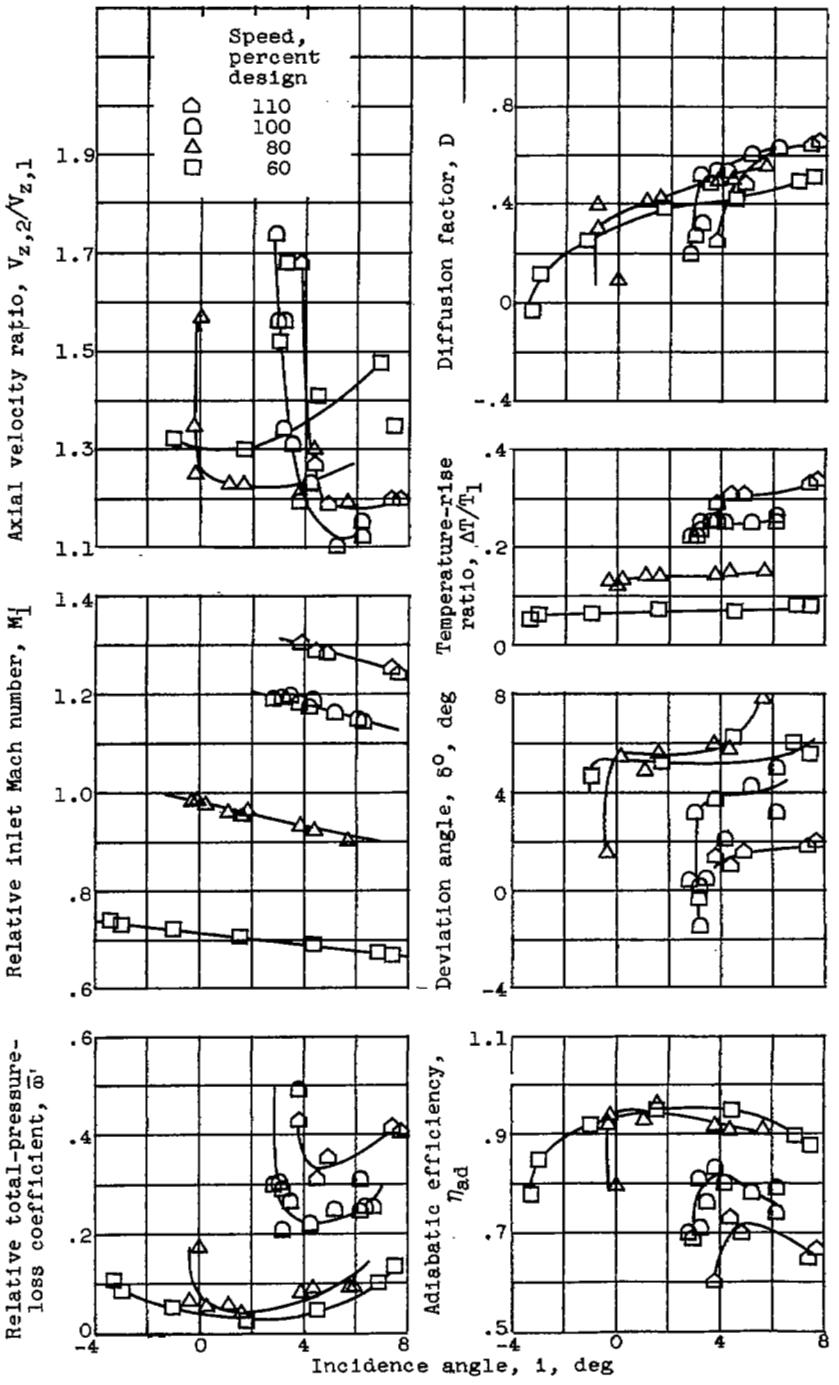

(b) 30-Percent-mass element; r_1 = 7.00 inches, r_2 = 6.92 inches.

Figure 8. - Continued. Blade-element characteristics.

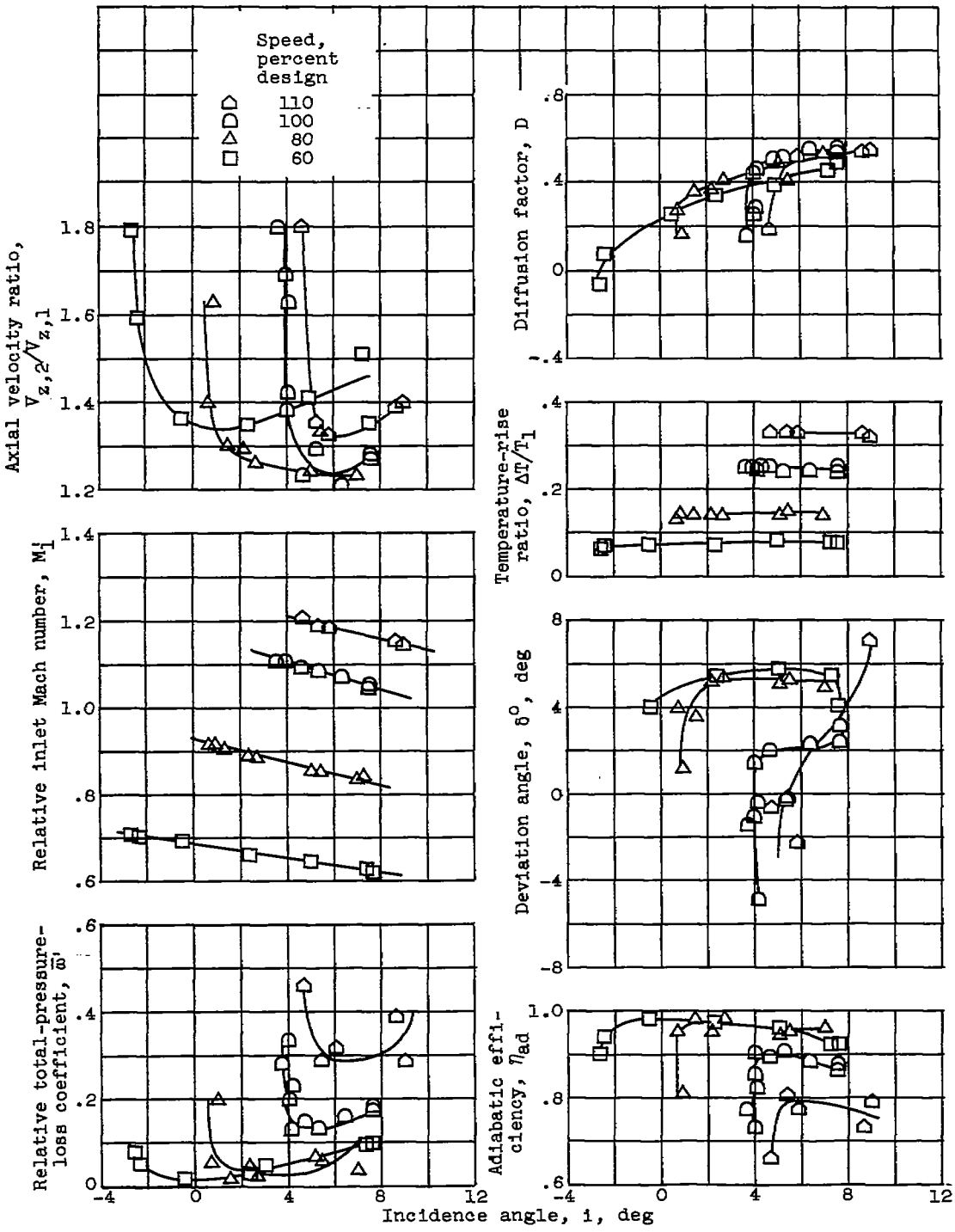

(c) 50-Percent-mass element; r_1 = 6.32 inches, r_2 = 6.45 inches.

Figure 8. - Continued. Blade-element characteristics.

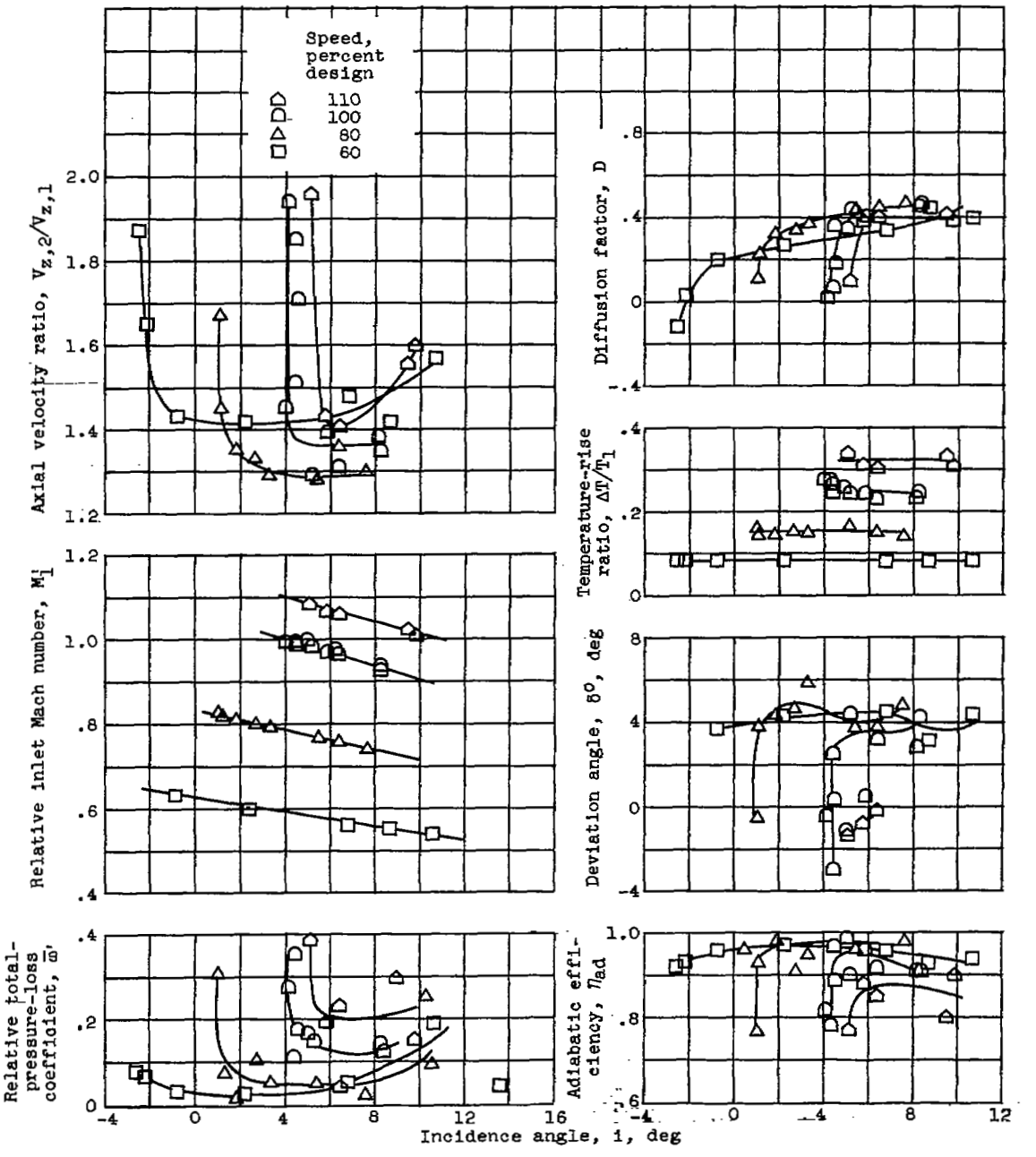

(d) 70-Percent-mass-element; r_1 = 5.53 inches, r_2 = 5.90 inches.

Figure 8. - Continued. Blade-element characteristics.

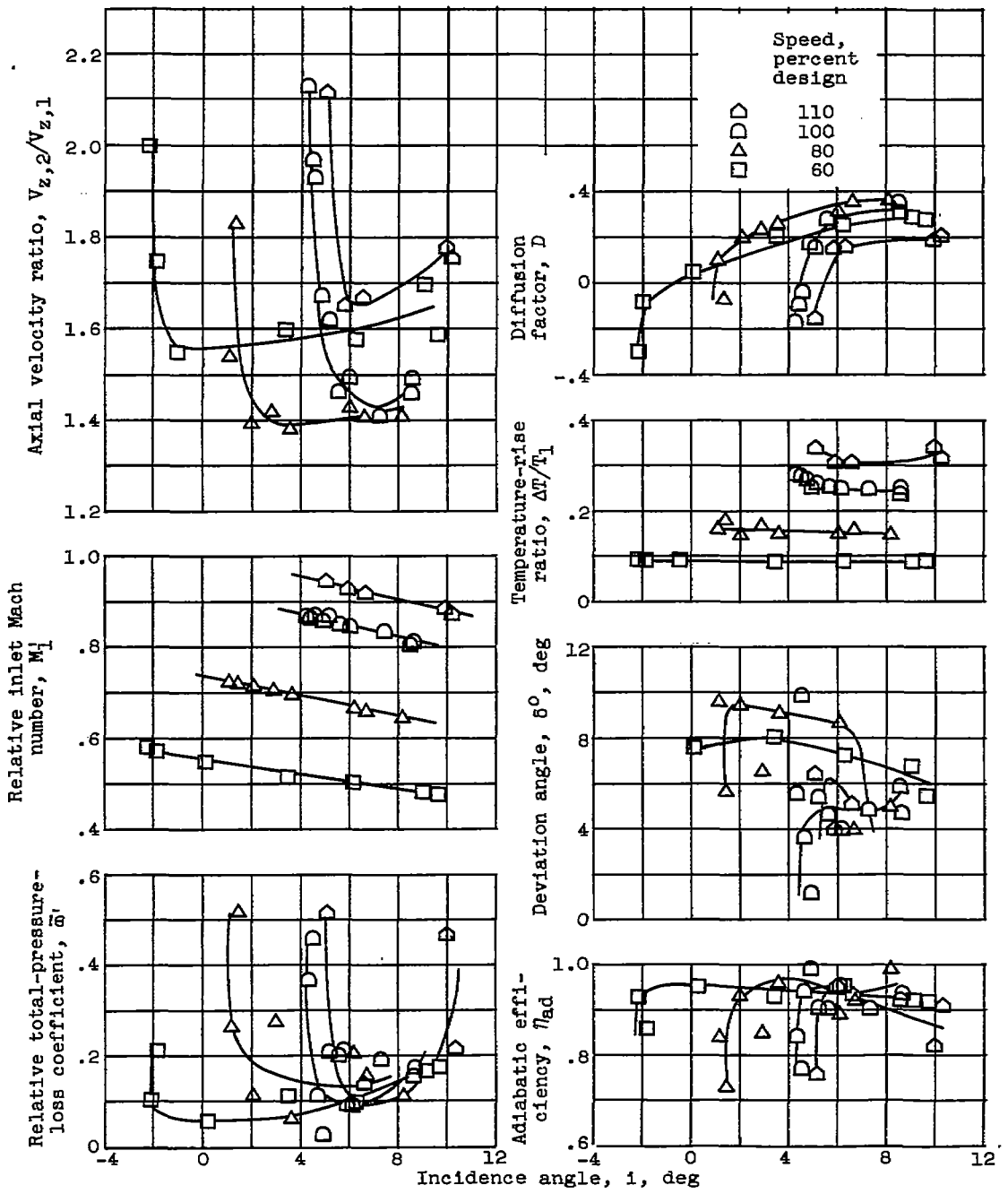

(e) 90-Percent-mass element; r_1 = 4.53 inches, r_2 = 5.27 inches.

Figure 8. - Concluded. Blade-element characteristics.

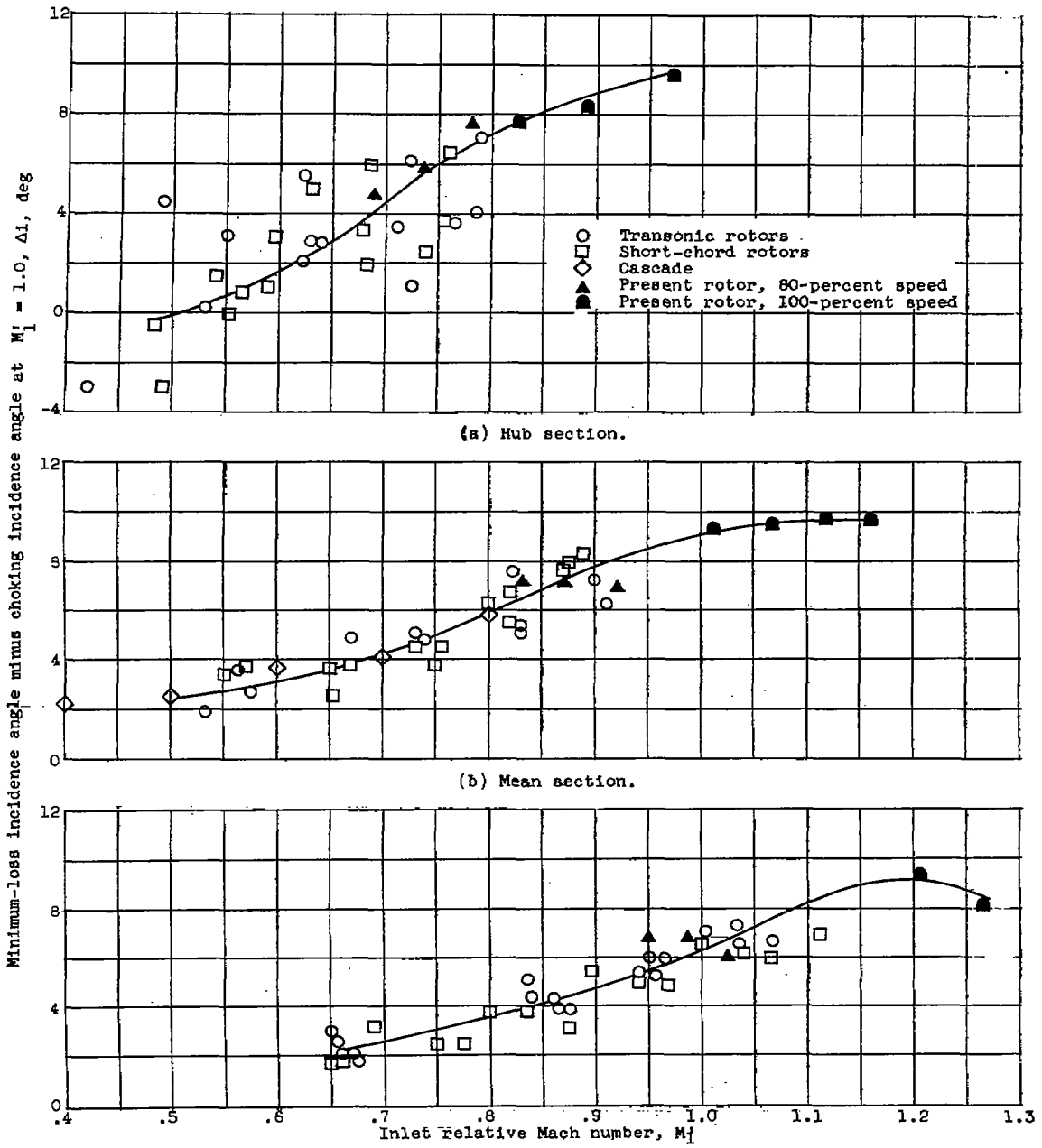

Figure 9. - Relation of minimum-loss and choking incidence angles at Mach 1.0 (ref. 2) with current data points added.

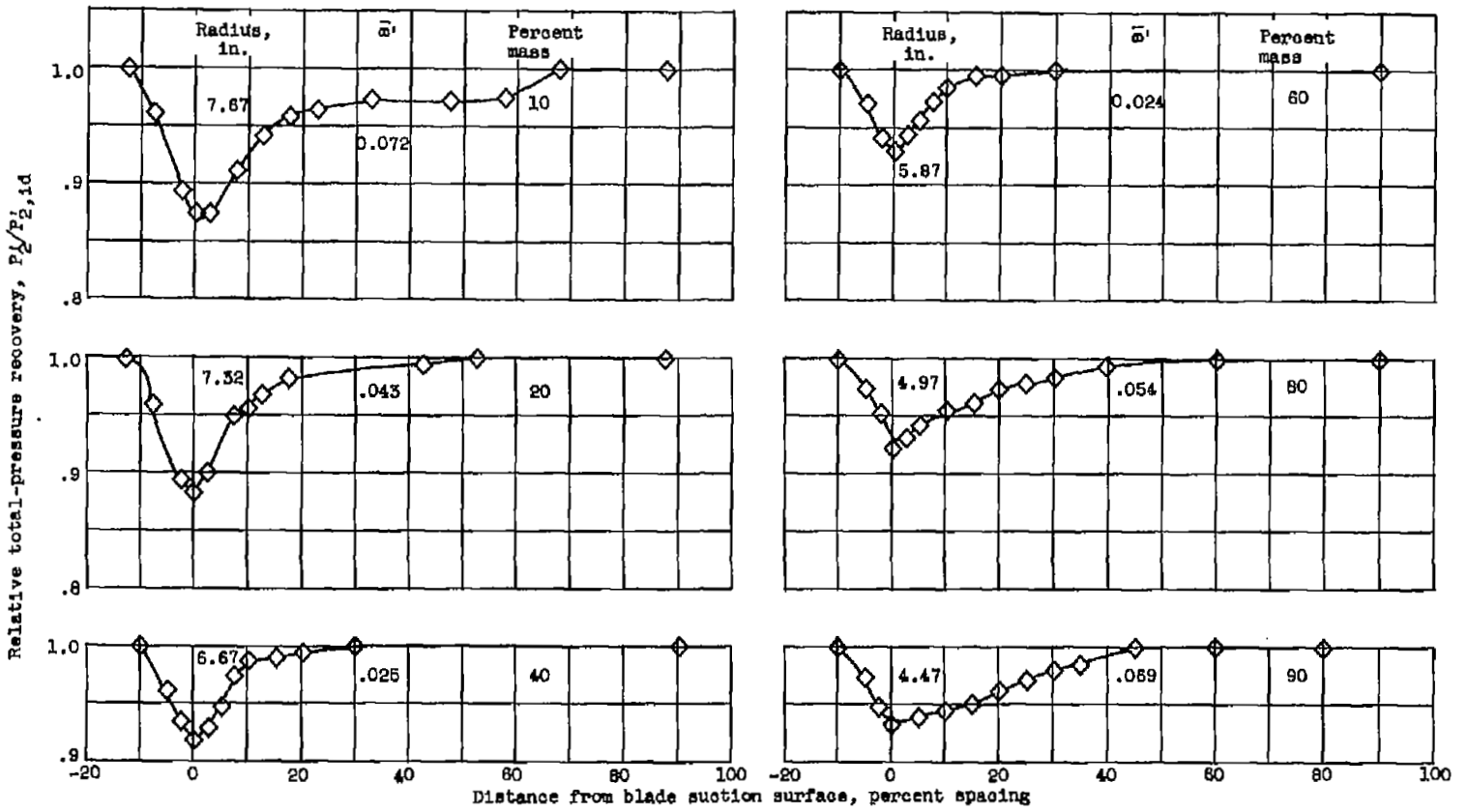

(a) Equivalent speed, 80-percent design. Near peak-efficiency weight flow.

Figure 10. - Circumferential total-pressure-recovery surveys from hot-wire traces.

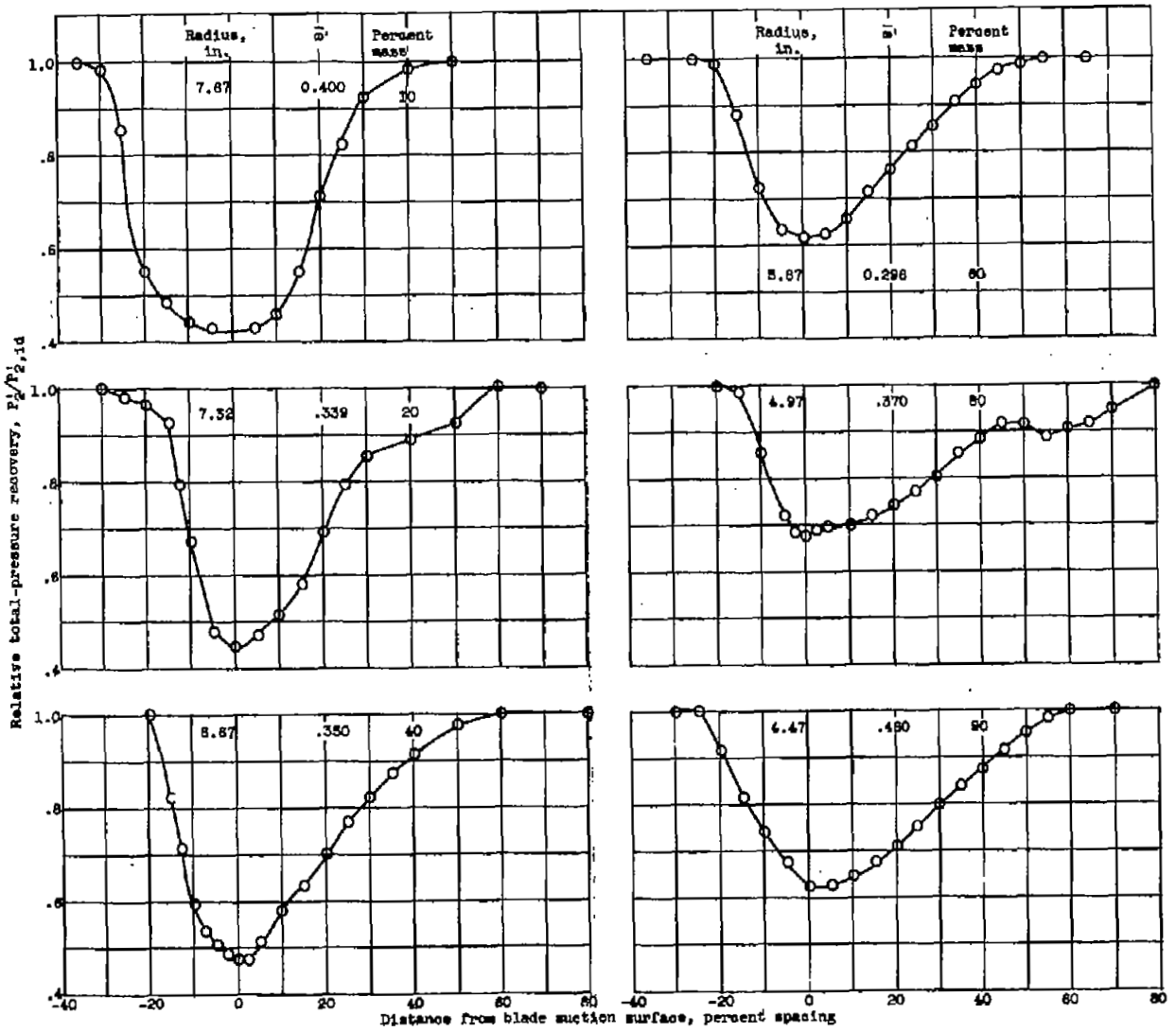

(b) Equivalent speed, 100-percent design. Open-throttle point (max. weight flow).

Figure 10. - Continued. Circumferential total-pressure-recovery surveys from hot-wire traces.

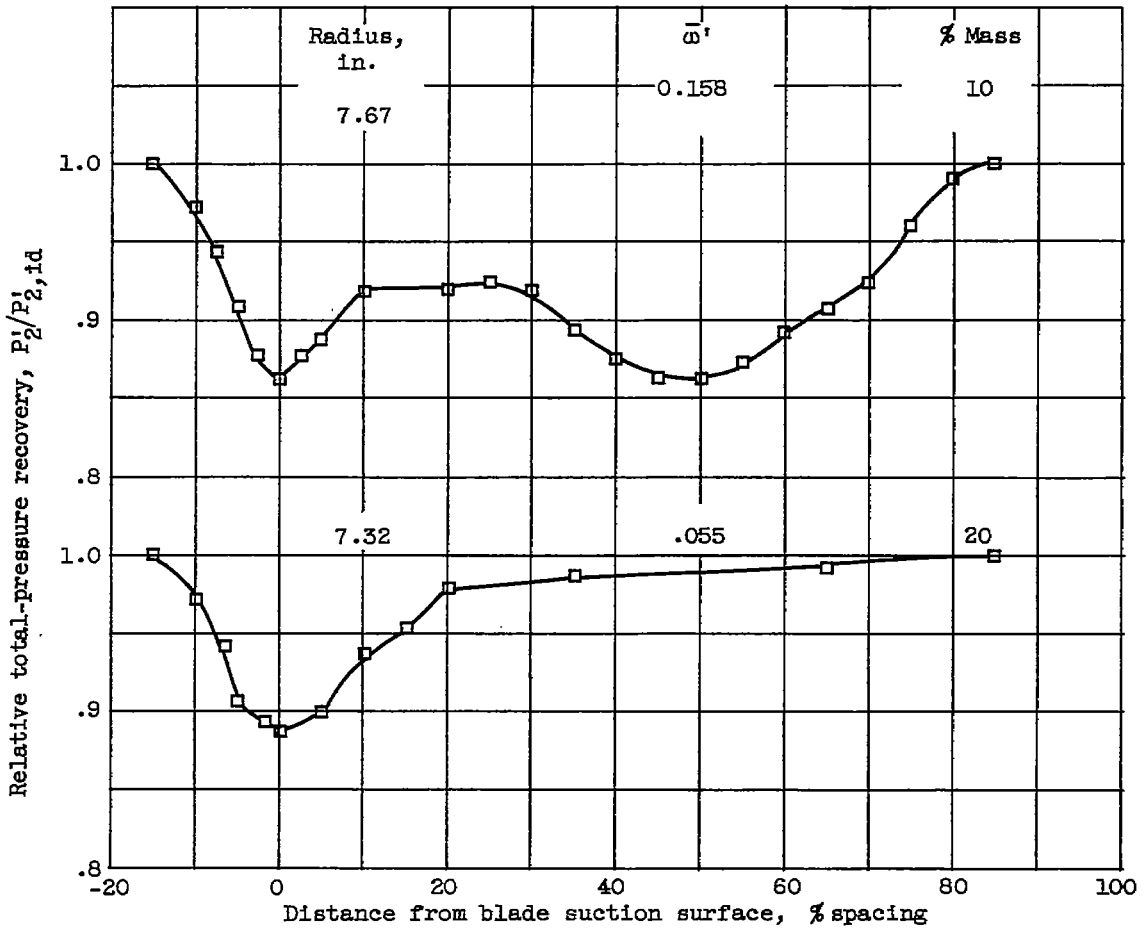

(c) Equivalent speed, 90-percent design. Near maximum weight flow.

Figure 10. - Concluded. Circumferential total-pressure-recovery surveys from hot-wire traces.

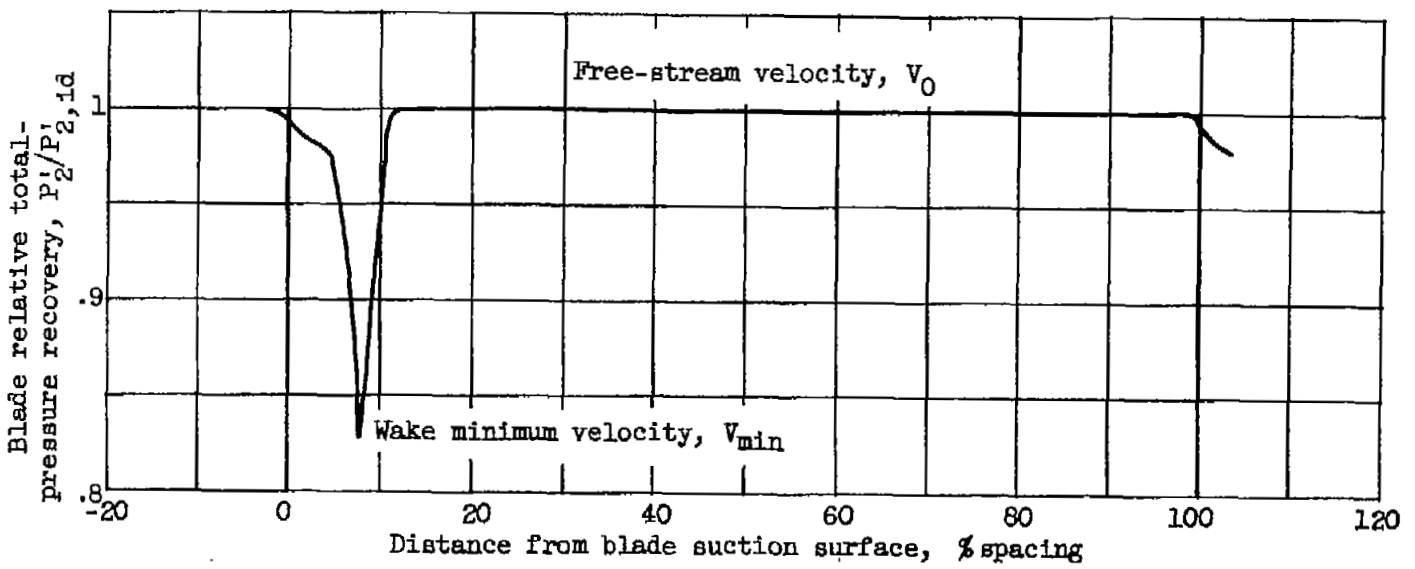

Figure 11. - Typical hot-wire trace behind a low-speed cascade, showing one blade wake immediately behind blade trailing edge.

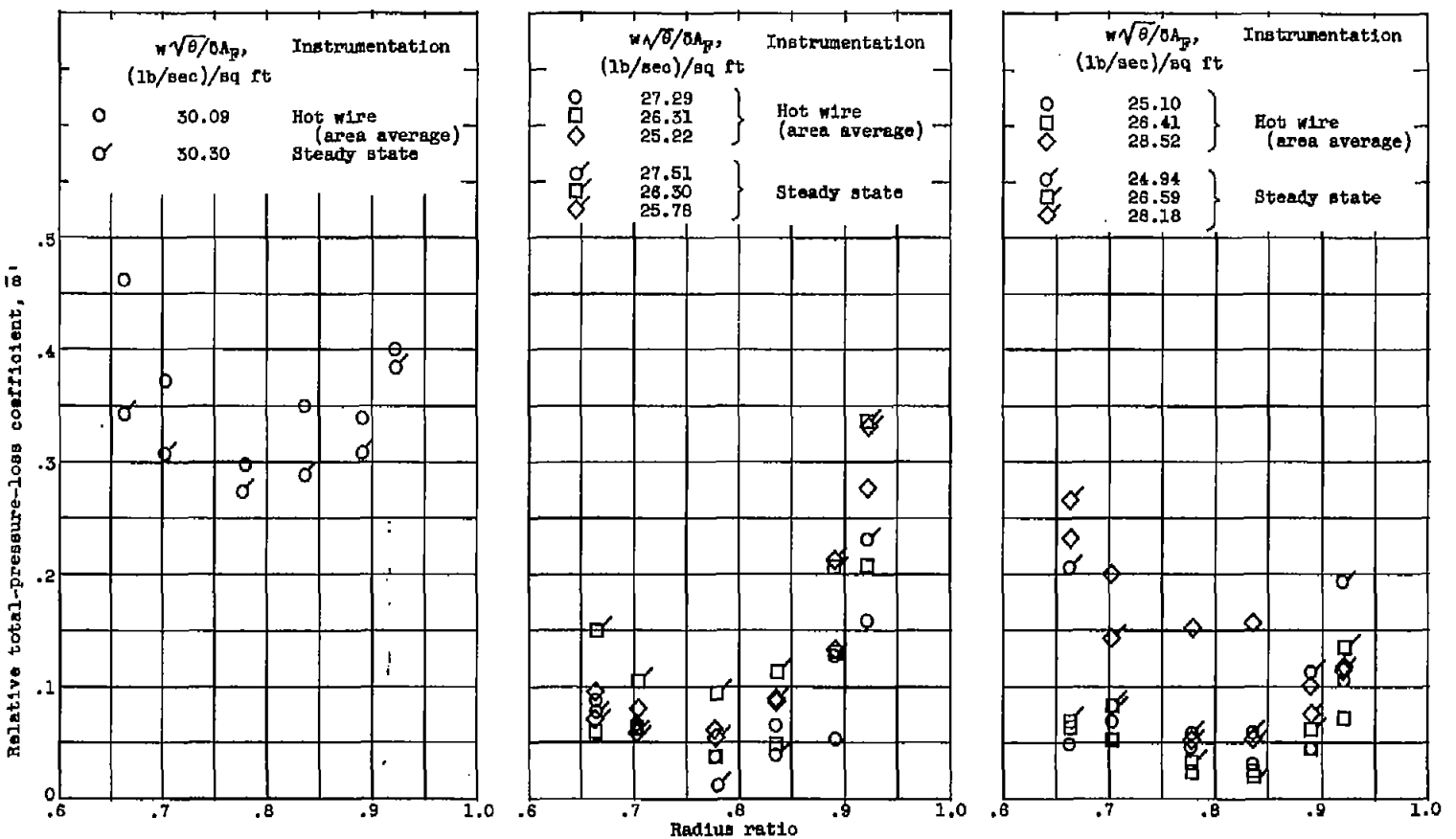

(a) Equivalent speed, 100-percent design. (b) Equivalent speed, 90-percent design. (c) Equivalent speed, 80-percent design.

Figure 12. - Comparison of element losses computed from hot-wire and from steady-state measurements for three different speeds.